



HAL
open science

A predictive model of organic acids separation by chromatography with strong anionic resins in sulfate form

Wuyang Zhong, Patrick Perre, Fanny Duval, Julien Lemaire

► **To cite this version:**

Wuyang Zhong, Patrick Perre, Fanny Duval, Julien Lemaire. A predictive model of organic acids separation by chromatography with strong anionic resins in sulfate form. *Journal of Chromatography A*, 2022, 1661, pp.462671. 10.1016/j.chroma.2021.462671 . hal-04403456

HAL Id: hal-04403456

<https://hal.science/hal-04403456v1>

Submitted on 18 Jan 2024

HAL is a multi-disciplinary open access archive for the deposit and dissemination of scientific research documents, whether they are published or not. The documents may come from teaching and research institutions in France or abroad, or from public or private research centers.

L'archive ouverte pluridisciplinaire **HAL**, est destinée au dépôt et à la diffusion de documents scientifiques de niveau recherche, publiés ou non, émanant des établissements d'enseignement et de recherche français ou étrangers, des laboratoires publics ou privés.

1 A predictive model of organic acids separation by chromatography with
2 strong anionic resins in sulfate form

3 Wuyang ZHONG, Patrick PERRE, Fanny DUVAL, Julien LEMAIRE*

4 Université Paris-Saclay, CentraleSupélec, Laboratoire de Génie des Procédés et Matériaux,
5 SFR Condorcet FR CNRS 3417, Centre Européen de Biotechnologie et de Bioéconomie (CEBB),
6 3 rue des Rouges Terres 51110 Pomacle, France

7 * Corresponding author.

8 Address : CEBB, CentraleSupélec, 3 rue des Rouges-Terres, 51110 Pomacle, France.

9 E-mail address: julien.lemaire@centralesupelec.fr

10 Tel : +33658045189

11 Keywords: Chromatography, Modeling, Strong anionic resin, CE/SE method, Langmuir
12 adsorption, ion-exchange

13 **Abstract**

14 Organic acids commonly have quite symmetrical chromatography profiles at low pH (< 1.5)
15 with strong anionic resins, but a significant tailing can be observed with succinic and citric
16 acids. Classical adsorption models, like the Langmuir model, fail to predict this behavior,
17 which can have a major influence on mean retention times and profile shapes, therefore on
18 chromatography performances.

19 A new retention model was developed to better predict organic acid separation with strong
20 anionic resin. This model combines a refined Langmuir adsorption model and an ion-
21 exchange model. Organic acid adsorption is assumed to be due to hydrogen bonding with
22 sulfate and hydrogen sulfate counter-anions on the resin. The adsorption capacity depends
23 mostly on molecular size: up to sixteen formic acid molecules could be adsorbed per
24 counter-anions, meanwhile only two succinic acid or one citric acid molecules could be
25 adsorbed.

26 This adsorption model was then embedded in a generic and accurate modeling approach
27 (continuous column with mass balance equations solved by the conservation
28 element/solution element (CE/SE) method). All parameters of this column model were
29 identified by fitting the simulation to experimental results (equilibrium curves and pulse
30 tests). Then, the column model was validated with original experimental results from a
31 binary mixture pulse test (formic and succinic acids). Results show that the simulations are
32 much more predictive for multi-component pulse tests, both in terms of profile shape and
33 retention time, which cannot be captured without considering ion-exchange.

34 Introduction

35 Chromatographic separation is a well-established technology in many domains, such as the
36 food and feed industry [1], pharmaceutical production [2], protein and enzyme purification
37 [3], and heavy metal separation [4]. Chromatography can separate or purify target
38 components, even with very close properties like stereoisomers, without using a large
39 amount of energy, chemicals, or solvent. For example, chromatography is often used to
40 separate sugars or organic acids from hemicellulose hydrolysates or fermentation broths [5].
41 These applications often require high purity, high recovery rate, and low operational costs
42 for economic reasons. Thus, chromatography is the ultimate solution when conventional
43 separation techniques such as distillation, liquid-liquid extraction, membrane filtration, or
44 crystallization are not sufficiently selective or consume too much energy, chemicals, or
45 solvent.

46 Preparative chromatography consists of pushing a mixture (generally liquid) through a
47 column filled with a porous solid phase using a mobile phase called the eluent. Its principle is
48 to separate different compounds according to their affinities towards both phases that
49 affect their travel speed and retention time inside the column. The solid phase can be
50 composed of dense or microporous resin beads. Hundreds of resin types exist on the market
51 to separate ions or organic molecules, depending on their structures and retention
52 mechanisms. Retention of a molecule on a resin surface often implies adsorption by Van Der
53 Waals forces owing to its hydrophobic matrix.

54 Ion-exchange resins are covered with counter-anions or counter-cations, making them
55 hydrophilic [6]. For instance, molecules such as sugars or organic acids can be separated by
56 different adsorption mechanisms (H bond, van der Waals force, chelation) with the counter-
57 ion fixed on the resin surface, and ionic compounds can be separated by ion-exchange or
58 Donnan exclusion effect. For example, strong anionic resins (coated with quaternary
59 ammonium groups) or weak anionic resins (coated with amine groups) are often used to
60 separate organic acids by interacting with their acid group.

61 However, the application of chromatography at an industrial scale is severely limited by its
62 low productivity, which impacts capital expenditures, and by how it dilutes separated
63 compounds, which impacts both capital and operational costs because further concentration
64 steps are required. To tackle these limiting factors, several dozen multi-column
65 chromatography processes have been developed over the last three decades, but their
66 development and tuning are difficult. Modeling the elution profile inside columns is a
67 valuable tool to make predictive simulations and optimize the performance of multi-column
68 chromatography systems. Further investigations and model development are still needed to
69 improve prediction accuracy, evidenced by continuing research activity in this field [7, 8, 9,
70 10].

71 For instance, our previous work found that outlet profiles of some organic acids have
72 uncommon tailing that cannot be explained by usual Langmuir adsorption models [11]. This
73 phenomenon was explained theoretically by considering the small fraction of organic acid
74 dissociated into anions ($< 1\%$ at pH below 1.5). Historically, this fraction was neglected, but it
75 can be strongly retained on resin ion-exchange sites [11]. A new model was then proposed
76 to better predict the behavior of organic acids with strong anionic resins. In addition,
77 Langmuir adsorption mechanisms were described in more detail, based on Honeywell
78 Universal Oil Products (Honeywell UOP) patent assumptions [12]. Mono-component

79 simulation of an organic acid profile was performed using a discontinuous column model
80 (Martin and Synge plate model [13]) and a finite difference method to solve differential
81 equations. Uncommon tailing of succinic and citric acid profiles was better predicted. This
82 model still needs to be adjusted and then validated with more experimental data and
83 improved for multi-component simulation.

84 Chromatography simulation is based on solving mass balances in the mobile phase
85 (convection-diffusion equations) and local exchanges with the stationary phase. It generally
86 results in a non-linear and coupled system of partial differential equations. The classical
87 numerical solving methods are finite element [14, 15, 16], finite difference [17,18], or finite
88 volume [19] for the spatial discretization, with an explicit or implicit time scheme. The CE/SE
89 (conservation element/solution element) method, proposed by NASA in 1995 [20], has been
90 applied for simulating explosions [21, 22], crystallization [23] and chemical reactions [24, 25].
91 It was first used to simulate chromatography with the Langmuir adsorption model in 2004
92 [26]. The CE/SE method allows simultaneous treatment of space and time integration. In the
93 case of packed bed chromatography [27], global trials of the CE/SE method showed a better
94 trade-off between accuracy, stability, and calculation speed than traditional methods using
95 an upwind scheme. Compared to conventional approaches, CE/SE method was proved, at
96 equivalent accuracy, to save the CPU time by 77% for the pseudo-linear system of glucose-
97 fructose separation, and by 96% for non-linear enantiomer separation [37].

98 The present work aims to improve the prediction of the outlet profile of different organic
99 acids and to confirm the role of ion-exchange with strong anionic resin. A more detailed
100 Langmuir adsorption model is proposed based on our previous theoretical work [11],
101 assuming that adsorption is due to a hydrogen bond between organic acids and sulfate
102 anions, as mentioned first in a UOP patent [12]. Experiments were performed first to identify
103 all model parameters (equilibrium constant, mass transfer coefficients, axial dispersion
104 coefficient), then to validate assumptions, and finally to check model prediction. In addition,
105 a continuous column model, solved by the CE/SE method, was developed to more accurately
106 simulate multi-component separation by chromatography. This new model tackles
107 discrepancies observed in the case of succinic or citric acid separation with strong anionic
108 resin.

109 2. Materials and methods

110 2.1 Experimental setup

111 The separation of organic acids by chromatography with strong anionic resin was studied
112 using a classical chromatography setup. Experimental devices and chemicals used in this
113 study are detailed in Tables 1 and 2.

114 The product or the eluent is fed at the top of column by the volumetric pump. The liquid
115 phase flows downwards in the column, while soluble compounds interact with the resin. The
116 output liquid goes through a pH and conductivity sensor, then a UV absorbance analyzer,
117 and finally is sampled by a fraction collector for offline analysis. All sensors and the fraction
118 collector are connected to a computer to monitor pH, conductivity, UV absorbance, and
119 sample collection.

120 The eluent was a H₂SO₄ solution at pH 1.5 (\approx 0.02 mol/L) for all experiments. For information,
121 its ionic strength is 0.0314 mol/L. Product pH was also adjusted at 1.5 to limit pH and
122 conductivity variation, and to keep a similar ionic strength during compound elution. The

123 on-line measurement of UV absorbance was used to select samples to analyze by HPLC. The
124 HPLC system (Ultimate 3000, Dionex) is equipped with a refractometer RI-101 (Shodex) at
125 35°C. The analytical column is an Aminex HPX-87H (Biorad) connected to a guard column
126 (Micro-Guard cartridge Biorad) kept at 45°C within an oven. The mobile phase is a 2 mmol/L
127 H₂SO₄ solution, prepared with Milli-Q water (Direct 8, Millipore).

128 The flowrate was set at 0.5 BV/h (BV represents the total bed volume, equal to 0.35 L),
129 corresponding to 3.10⁻⁴ m/s interstitial flow velocity (Re_p = 6.6). The internal column
130 diameter was 2.5 cm, and the bed length was 70 cm. A jacketed column linked to a
131 thermostatic bath was used to maintain the temperature at 25°C. The column was filled with
132 the strong anion resin DIAION UMA 150, functionalized with trimethylamine groups (type 1),
133 manufactured by Mitsubishi Chemical, whose characteristics are summarized in Table 3. The
134 resin is supplied in Cl⁻ form, but it was put in sulfate form before running experiments by
135 using the following procedure: 2 BV of 1 mol/L Na₂SO₄ solution was fed into the column at 1
136 BV/h, then 8 BV of eluent was fed to wash the bed resin and reach pH equilibrium.

137 The bed porosity was measured by a pulse test with 10 mL 1 mol/L Na₂SO₄ solution eluted at
138 1 BV/h. The porosity was estimated between 0.39 and 0.41, which corresponds to the range
139 given by the resin manufacturer (Table 3). Finally, the extra-column volume (in tubes, valves,
140 sensors, etc.) was measured by performing a similar pulse test without the chromatography
141 column. It was estimated around 0.05 BV (15 mL). All chromatographic profiles were
142 corrected by removing this extra-column volume from the eluted volume.

143 2.2 Determination of transfer and axial dispersion coefficient

144 A pulse test consists of injecting a small volume of product (0.05 BV) followed by the eluent
145 at a constant flow rate until all compounds leave the column. It is one of the most common
146 methods used in chromatography to study compound retention and dispersion along the
147 column. A pulse test was chosen in our study to determine physical properties such as
148 adsorption isotherm, mass transfer coefficients, bed porosity and extra-column volume.

149 During pulse tests, component concentrations at column output are plotted as a function of
150 the eluted volume. The curve obtained is usually called a chromatographic profile, which
151 looks like a peak more or less wide and symmetric. This profile is mainly characterized by its
152 mean retention volume V_R and its standard deviation σ :

$$V_R = \int_0^{\infty} V \cdot c \cdot dV / \int_0^{\infty} c \cdot dV \quad (1)$$

$$\sigma^2 = \int_0^{\infty} V^2 \cdot c \cdot dV / \int_0^{\infty} c \cdot dV - V_R^2 \quad (2)$$

153 where V is the eluted volume (in BV), and c is the component concentration in the mobile
154 phase at column output (concentration unit does not matter).

155 The peak width depends almost on axial dispersion and mass transfer resistance while the
156 component passes through the column. The volume of product fed into the column (< 0.05
157 BV) is small enough to have a negligible influence on the shape of the pulse test profile.
158 Dead volumes were minimized to limit their influence on dispersion. The global dispersion is
159 usually characterized by the height equivalent to a theoretical plate (HETP) as a function of
160 V_R , σ^2 and the bed length L :

$$HETP = \frac{L \cdot \sigma^2}{V_R^2} \quad (3)$$

161 The van Deemter curve [28] describes the relationship between HETP (inversely proportional
 162 to the global dispersion) and the interstitial velocity v (in $\text{m}\cdot\text{s}^{-1}$). This curve is estimated
 163 experimentally by plotting the HETP of component profiles obtained at different flowrates
 164 during the pulse test (Fig. 1).

165 One of the most known versions of the van Deemter equation reads as:

$$HETP = A + \frac{B}{v} + C \cdot v \quad (4)$$

166 This equation considers that the global dispersion has three main causes: the mechanical
 167 dispersion (A term), the molecular diffusion (B term), and the mass transfer resistance (C
 168 term), as depicted in Figure 1. The mathematical expressions to obtain the values of A , B ,
 169 and C are important for prediction purposes. The original article by van Deemter [28] gives
 170 the following expressions:

$$A = 2 \cdot \beta \cdot d_p \quad B = 2 \cdot \frac{D_m}{\tau} \quad C = 2 \cdot \left[\frac{\varepsilon/\alpha}{(1 + F/K_j)^2} \right] \quad (5)$$

171 where β is a packing factor that equals 1 for a homogeneous packed bed, d_p is the mean
 172 particle diameter (in m), D_m is the molecular diffusion coefficient (in $\text{m}^2\cdot\text{s}^{-1}$), τ is the bed
 173 tortuosity, ε is the bed porosity, $F = \varepsilon/(1 - \varepsilon)$ is the volumetric ratio of mobile phase to
 174 stationary phase, K_j is the linear equilibrium constant (concentration ratio between
 175 stationary and mobile phase), and α is the liquid-side local mass transfer coefficient (s^{-1}).

176 Within narrow operating conditions of preparative chromatography (flowrate between 0.5
 177 and 2 BV/h), van Deemter curves are almost linear over the whole interstitial velocity range.
 178 Thus, the most simple version of van Deemter equation was sufficient to describe
 179 experimental results and estimate its coefficients.

180 From experimental points, the range of C can be estimated quite accurately by linear
 181 regression, then α range can be deduced from previous equation. A and B are difficult to
 182 estimate separately because of the lack of experimental points in the non-linear part of van
 183 Deemter curve. However, in the present modelling work, only axial dispersion coefficient D is
 184 required, and it can be expressed as the sum of molecular diffusion and mechanical
 185 dispersion, according to the following equation:

$$D = \frac{D_m}{\tau} + \beta \cdot d_p \cdot v = \frac{A}{2} \cdot v + \frac{B}{2} \quad (6)$$

186 Thus, the range of D can be estimated quite accurately from the experimental points by
 187 fitting the van Deemter equation with the least squares method, while considering the range
 188 of C previously estimated by linear regression.

189 2.3 Physical formulation at the bed level

190 2.3.1 Mass balance

191 Two types of unidimensional column model are often used to describe the mass transfer
 192 inside a chromatography column [13]:

- 193 • Continuous models, solved by usual finite methods, where the column is discretized
 194 into a large number of very small elements. In this case, the axial dispersion depends
 195 on the axial dispersion coefficient D and the global mass transfer coefficient k_a .
 196 • Discontinuous models where the chromatography column is assimilated to a plate
 197 column. Each theoretical plate acts as a perfectly stirred reactor. In this case, the
 198 axial dispersion becomes an emerging property of the theoretical plate number N .

199 Discontinuous models, easy to code and to solve, require low CPU time. However, because
 200 the axial dispersion is an indirect effect of the theoretical plate number N , this model
 201 imposes the same axial dispersion for all compounds. Thus, this model is not appropriate for
 202 multi-component chromatography simulation if their axial dispersion coefficients D are not
 203 similar. That is the reason why a continuous model was chosen in the present work.

204 At the level of the chromatography column (Fig. 2), the local 1-D mass balance of one
 205 component j in the mobile phase, for a section of extension ∂x , can be expressed as two
 206 mass balances for liquid side and solid side:

$$\varepsilon \frac{\partial c_j}{\partial t} + \varepsilon \cdot v \frac{\partial c_j}{\partial x} = \varepsilon \cdot D \frac{\partial^2 c_j}{\partial x^2} + \varepsilon \cdot R_j^{a \leftrightarrow b} - (1 - \varepsilon) \cdot R_j^{l \leftrightarrow s} \quad (7)$$

$$\frac{\partial q_j}{\partial t} = R_j^{l \leftrightarrow s} \quad (8)$$

207 where c_j is the concentration of component j in the mobile phase (in $\text{mol} \cdot \text{m}^{-3}$), D is the axial
 208 dispersion coefficient (in $\text{m} \cdot \text{s}^{-2}$), v is the interstitial velocity (in $\text{m} \cdot \text{s}^{-1}$), $R_j^{a \leftrightarrow b}$ is the mass
 209 variation of component j due to acid–base reactions (in $\text{mol} \cdot \text{m}^{-3} \cdot \text{s}^{-1}$), $R_j^{l \leftrightarrow s}$ is the mass
 210 exchange of component j between the mobile phase and the stationary phase (in
 211 $\text{mol} \cdot \text{m}^{-3} \cdot \text{s}^{-1}$), and q_j is the concentration of component j in the stationary phase (in $\text{mol} \cdot \text{m}^{-3}$).

212 The $R_j^{a \leftrightarrow b}$ term is due to the acid–base reactions in the mobile phase between SO_4^{2-} and
 213 HSO_4^- anions, organic acid HA and its conjugate base A^- , and H^+ cations. When the mobile
 214 phase goes through the column, organic acids HA can be retained by Langmuir adsorption;
 215 meanwhile, A^- can be exchanged by SO_4^{2-} or HSO_4^- anions on resin sites. As the
 216 concentration ratio between acid and basic compounds changes in the mobile phase, the
 217 acid–base reactions tend to restore equilibrium by transforming the acid into a base or the
 218 inverse.

219 Finally, to avoid any $R_j^{a \leftrightarrow b}$ term, mass balances in the mobile phase were written for the
 220 total content of each organic acid A ($c_A^{\text{tot}} = c_{\text{A}^-} + c_{\text{HA}}$), the total sulfate content SO_4
 221 ($c_{\text{SO}_4}^{\text{tot}} = c_{\text{SO}_4^{2-}} + c_{\text{HSO}_4^-}$) and the total acid content H ($c_{\text{H}}^{\text{tot}} = c_{\text{H}^+} + c_{\text{HA}} + c_{\text{HSO}_4^-}$). These
 222 balances are not affected by acid–base reactions. Then, the concentration of each
 223 compound can be estimated using the equilibrium constant of each acid–base reaction.
 224 Indeed, these reactions are assumed to always be at an equilibrium state because they are
 225 considered to be much faster than all other phenomena.

226 The mass exchange $R_j^{l \leftrightarrow s}$ between the mobile phase and stationary phase depends on the
 227 adopted mass transfer model. With instantaneous mass transfer model, concentrations q_j in
 228 the stationary phase are assumed to be in equilibrium with concentrations c_j in the mobile
 229 phase. In this case, it is not necessary to estimate $R_j^{l \leftrightarrow s}$ because concentrations q_j can be
 230 deduced directly from concentrations c_j by solving the equilibrium equations system. With a

231 non-instantaneous mass transfer model, a new equation is needed to estimate $R_j^{l \leftrightarrow s}$, which
232 also depends on equilibrium equations between the mobile and stationary phase.

233 In a previous work [11], the instantaneous mass transfer model was adopted with a
234 discontinuous model, as the influence of mass transfer resistance can be considered directly
235 in the theoretical plate number N that summarizes the global effect of all dispersion
236 mechanisms.

237 In the present work, a non-instantaneous mass transfer model was chosen to consider
238 compounds with different mass transfer resistances. Mass transfer resistance between the
239 mobile and stationary phase is driven by molecular diffusion and hydrodynamic properties at
240 the interface (summarized in the Sherwood number, depending on Reynolds and Schmidt
241 numbers). The lumped model was chosen to estimate the mass exchange $R_j^{l \leftrightarrow s}$ from the
242 global mass transfer coefficient k_{a_j} of component j (in s^{-1}) between the mobile phase and
243 the stationary phase, due to diffusion inside resin and at its interface [29]:

$$R_j^{l \leftrightarrow s} = k_{a_j} \cdot (q_j^{eq}(c) - q_j) \quad (9)$$

244 where q_j^{eq} represents the theoretical concentration of component j in the stationary phase
245 (in $\text{mol} \cdot \text{m}^{-3}$), which would be in equilibrium with the mobile phase. This equilibrium is
246 calculated from the concentration of all components in the mobile phase by solving all
247 equilibrium equations (adsorption, ion-exchange, and acid–base reactions).

248 The mass exchange $R_j^{l \leftrightarrow s}$ can also be expressed at the liquid side, as:

$$R_j^{l \leftrightarrow s} = \alpha_j \cdot (c_j - c_j^i) \quad (10)$$

249 where c_j^i is the concentration of the component j at the interface (in $\text{mol} \cdot \text{m}^{-3}$).

250 Thus, k_{a_j} can be estimated from the α_j value by assuming a linear equilibrium, whose
251 coefficient K_j is estimated from the adsorption isotherm of component j (cf. section 2.3.2).

$$q_j = K_j * c_j^i \quad q_j^{eq} = K_j * c_j \quad k_a = \frac{\alpha_j \cdot (c_j - c_j^i)}{(q_j^{eq} - q_j)} = \frac{\alpha_j}{K_j} \quad (11)$$

252 2.3.2 Adsorption mechanisms

253 Counter-anions SO_4^{2-} or HSO_4^- cover the surface of strong anionic resin in sulfate form (Fig.
254 3). Their proportion depends on ion-exchange equilibrium and their concentration in the
255 mobile phase. The adsorption mechanism of organic acid on this type of resin is not well
256 documented in the literature. UOP patents [30, 31] suggested that the molecular form of
257 organic acid was retained only on counter-anions HSO_4^- and SO_4^{2-} . Lemaire *et al.* [11]
258 developed this hypothesis in their model, assuming that the interaction was probably
259 hydrogen bonding between the acid hydrogen atom of organic acids and the lone electron
260 pairs of sulfate and hydrogen sulfate oxygen atoms.

261 A Langmuir model is generally used to describe adsorption on chromatography resins, which
262 involves several assumptions [32]:

- 263 1. The surface containing adsorption sites is perfectly flat with no corrugation,
- 264 2. All adsorption sites are energetically equivalent,
- 265 3. Only mono-layer coverage occurs,

266 4. No interaction occurs between molecules adsorbed on adjacent sites.

267 As shown in Figure 3, each SO_4^{2-} or HSO_4^- contains eight lone electron pairs, so up to eight
268 hydrogen bonds can be theoretically observed on each anion. As an improvement compared
269 to previous works [11], this feature was directly integrated into the adsorption equation in
270 the present work. As a first approximation, the adsorption sites on SO_4^{2-} and HSO_4^- were
271 assumed to be similar. Thus, instead of writing two adsorption equations for SO_4^{2-} and HSO_4^-
272 separately, the total concentration of SO_4^{2-} and HSO_4^- in the stationary phase, called $q_{\text{SO}_4}^{\text{tot}}$ (in
273 mol/L), was used. In the case of a single component model, the Langmuir equilibrium model
274 for component j was described as:

$$q_j = \frac{N_{\text{tot}} \cdot q_{\text{SO}_4}^{\text{tot}} \cdot k_{s_j} \cdot c_j}{1 + N_j \cdot k_{s_j} \cdot c_j} \quad (12)$$

275 where N_{tot} is the number of lone electron pairs on each counter-anion ($N_{\text{tot}} = 8$), k_{s_j} is the
276 adsorption constant of component j , and N_j is the number of lone electron pairs occupied by
277 each adsorbed molecule.

278 In the case of a multi-component model, the competitive Langmuir equilibrium model for m
279 components can be described as:

$$q_j = \frac{N_{\text{tot}} \cdot q_{\text{SO}_4}^{\text{tot}} \cdot k_{s_j} \cdot c_j}{1 + \sum_{i=1}^m N_i \cdot k_{s_i} \cdot c_i} \quad (13)$$

280 The value of $q_{\text{SO}_4}^{\text{tot}}$ can be estimated from the value of the ion-exchange resin capacity q_{max} ,
281 which is the concentration of quaternary ammonium groups RMe_3N^+ . The resin supplier
282 provides an estimation (ca. 2.3 eq/L where eq corresponds to the equivalent molar charge
283 amount). This value was checked by mixing a given volume of resin in OH^- form with a given
284 volume of H_2SO_4 solution whose concentration is known. The titration of residual acid
285 concentration in the solution enabled estimating the initial OH^- concentration in resin ($2.1 \pm$
286 0.2 eq/L).

287 Equilibrium curves of additional organic acids, determined by frontal analysis, are currently
288 in progress in our laboratory. This dataset is intended to refine the competitive Langmuir
289 equilibrium model. So far, these additional results are consistent and will be the object of
290 another paper. Equilibrium curves enable us to estimate Langmuir model coefficients (N and
291 k_s) by fitting the model to experimental points. As the N and k_s values are correlated in the
292 linear zone of equilibrium curves, their estimation can be quite inaccurate when it is
293 impossible to obtain sufficient experimental points in the non-linear zone. Consequently, N
294 and k_s are given in Table 4 with their uncertainty range. Because N represents the number
295 of lone electron pairs occupied by each adsorbed molecule, N was assumed afterward to be
296 equal to only rounded values that could be explained physically. When the experimental
297 range of N can include two possibilities (for formic and succinic acids), two corresponding
298 ranges of the k_s value were identified.

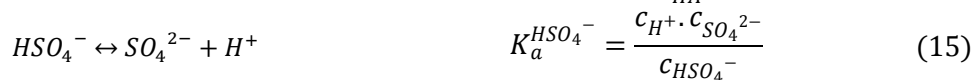
299 According to the Langmuir adsorption model and N estimation from Table 4, formic, succinic,
300 and citric acids seem to occupy a different number N of lone electron pairs on oxygen atoms
301 of sulfate or hydrogen sulfate counter-anions. The values are rather consistent with their
302 different molecular size and the number of carboxylic acid groups (Fig. 4).

303 Citric acid occupies more adsorption sites, most likely because of its large molecular size,
 304 which hinders access to free lone pairs, and its three carboxylic acid groups that can make H
 305 bonds with up to three lone pairs. $N = 8$ corresponds to only one citric acid molecule per
 306 sulfate or hydrogen sulfate counter-anion (all eight lone pairs occupied: H-bond or cluttered).
 307 Inversely, $N = 0.5$ or 1 for formic acid, which is the smallest acid and has only one carboxylic
 308 acid group. It corresponds to one or two formic acid molecules per lone pairs (none
 309 cluttered and only single H-bonds). The formation of formic acid dimers could explain that
 310 up to two molecules can occupy the same adsorption site [33]. Succinic acid is an
 311 intermediate case because of its medium size and two carboxylic acid groups. $N = 4$ or 8
 312 corresponds to one or two succinic acids per sulfate or hydrogen sulfate counter-anions
 313 (four or eight lone pairs occupied).
 314 k_s values of formic, succinic, and citric acid are quite similar and correspond to the strength
 315 of the H-bond between their carboxylic acid group and lone electron pairs of sulfate or
 316 hydrogen sulfate counter-anions. Their value has been refined further in the present work to
 317 remove the possible influence of ion-exchange that may have caused k_s overestimation.

318 2.3.3 Ion-exchange mechanisms

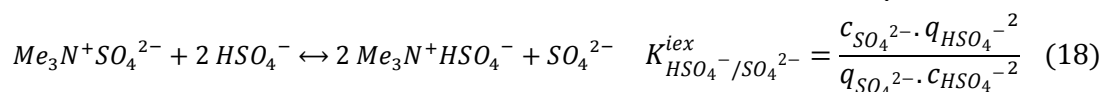
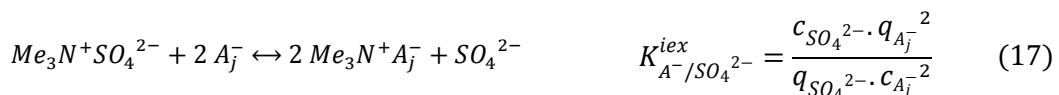
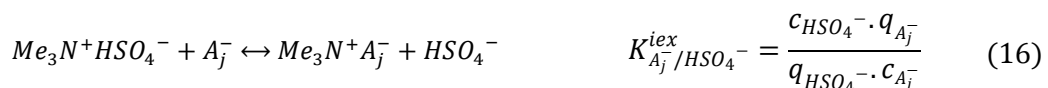
319 In the present model, ion-exchange was also considered to explain the retention of some
 320 organic acids with a particular chromatographic profile (large tailing) with strong anionic
 321 resin in sulfate form. Indeed, despite the very low dissociation of organic acids at pH below 2,
 322 a small concentration of corresponding organic anions could greatly influence their profile in
 323 the case of a very strong affinity for resin ion-exchange sites.

324 In the mobile phase, organic acid HA and hydrogen sulfate anion HSO_4^- can dissociate into its
 325 corresponding conjugate base A^- or SO_4^{2-} and one proton H^+ . The corresponding acid–base
 326 equilibria can be written as follow:



327 In the present model, usual pKa values of formic, succinic, and citric acids and hydrogen
 328 sulfate at 20 °C (operating temperature) were considered: 3.76, 4.16, 3.13, and 1.99,
 329 respectively.

330 Organic anions A_j^- can replace HSO_4^- or SO_4^{2-} counter-anions on quaternary ammonium
 331 ion-exchange sites. Ion-exchange reactions correspond to the following equilibria:



332 where K_{X^-/Y^-}^{iex} is the ion-exchange coefficient of anions X^- by anions Y^- on resin sites.

333 In the stationary phase, the concentration of ion-exchange sites q_{max} is always conserved:

$$q_{max} = 2 \cdot q_{SO_4^{2-}} + q_{HSO_4^-} + \sum_j q_{A_j^-} \quad (19)$$

334 All corresponding equilibrium constants can be deduced from resin manufacturer data listed
 335 in the appendices [34, 35], which provides the value of K_{X^-/OH^-}^{eq} between many anions X^-
 336 and OH^- .

337 2.4 Computational strategy

338 As detailed in the introduction, several computational methods could be used to solve the
 339 system of equations in space and in time. The CE/SE method was chosen in the present work
 340 for its ability to deal with space and time integrals simultaneously. The integral is calculated
 341 between normal mesh points and intermediate mesh points, and it takes two integrals to
 342 move one step forward in space or time.

343 This method is based on Gauss's divergence theorem [36]. In the case of a 1D space model, it
 344 is also called Green's theorem. For a partial differential equation (PDE) like:

$$\frac{\partial u}{\partial t} + \frac{\partial f}{\partial x} = p \quad (20)$$

345 Green's theorem tells us that the line integral along a closed curve ∂C of a function equals
 346 the integral of the derivative over the corresponding plane region ∂D :

$$\oint_{\partial C} (-u \cdot dx + f \cdot dt) = \iint_{\partial D} \left(\frac{\partial u}{\partial t} + \frac{\partial f}{\partial x} \right) \cdot dx \cdot dt = \iint_{\partial D} p \cdot dx \cdot dt \quad (21)$$

347 Figure 5 shows the space and time discretization used and the mesh points where all
 348 variables are estimated. By definition, the solution element SE (j,n) is the gray space-time
 349 interior region centered at point A (j,n). It includes a horizontal line segment, a vertical line
 350 segment, and their immediate neighborhood points (B, D, F). In this solution element, we
 351 chose to approximate u and f values by a first-order Taylor formula from its center point A
 352 (j,n):

$$u^*(x, t) \sim u_j^n + u_{x_j}^n \cdot (x - x_j) + u_{t_j}^n \cdot (t - t_n) \quad (22)$$

$$f^*(x, t) \sim f_j^n + f_{x_j}^n \cdot (x - x_j) + f_{t_j}^n \cdot (t - t_n) \quad (23)$$

353 where $u_{x_j}^n$ and $f_{x_j}^n$ correspond to the space derivative of u and f at the mesh point (j,n), and
 354 $u_{t_j}^n$ and $f_{t_j}^n$ correspond to the time derivative of u and f at the mesh point (j,n).

355 A zero-order Taylor formula was chosen to approximate the source term p , which means
 356 that p was treated as a constant in each solution element:

$$p^*(x, t) \sim p_j^n \quad (24)$$

357 The conservation element CE (j,n) corresponds to the rectangle FADE (blue) and ABCD
 358 (green), where the source term p was consequently considered equal at mesh points A, B, D,
 359 and F, but different at mesh points C ($p_{j-1/2}^{n-1/2}$) and E ($p_{j+1/2}^{n-1/2}$).

360 Finally, Green's theorem applied within the rectangle FBCE (blue + green) by approximating
 361 u , f and p leads to the following explicit equation that enabled u_j^n to be estimated from
 362 values of u , f and p at the previous semi-time step:

$$u_j^n = \frac{1}{2} \left[u_{j+\frac{1}{2}}^{n-\frac{1}{2}} + u_{j-\frac{1}{2}}^{n-\frac{1}{2}} \right] - s_{j+\frac{1}{2}}^{n-\frac{1}{2}} + s_{j-\frac{1}{2}}^{n-\frac{1}{2}} + \frac{\Delta t}{4} \cdot \left(p_{j+\frac{1}{2}}^{n-\frac{1}{2}} + p_{j-\frac{1}{2}}^{n-\frac{1}{2}} \right) \quad (25)$$

363 where

$$s_{j\pm\frac{1}{2}}^{n-\frac{1}{2}} = \left(\frac{\Delta t}{2 \cdot \Delta x} \right) \cdot f_{j\pm\frac{1}{2}}^{n-\frac{1}{2}} + \left(\frac{\Delta x}{8} \right) \cdot u_{x,j\pm\frac{1}{2}}^{n-\frac{1}{2}} + \left(\frac{\Delta t^2}{8 \cdot \Delta x} \right) \cdot f_{t,j\pm\frac{1}{2}}^{n-\frac{1}{2}} \quad (26)$$

364 In the case of chromatography convection-diffusion equation, the CE/SE method can be
365 applied to solve the mass balance in the mobile phase by defining:

$$f = v \cdot c - D \cdot \frac{\partial c}{\partial x} \quad u = c \quad p = -\frac{(1 - \varepsilon)}{\varepsilon} \cdot k_a \cdot (q^{eq} - q) \quad (27)$$

366 As a consequence, f , u_t , f_x , then f_t can be deduced from u_x at the mesh point (j,n):

$$f = v \cdot u - D \cdot u_x \quad f_x = \frac{\partial f}{\partial u} \cdot \frac{\partial u}{\partial x} = \left(v \cdot \frac{\partial u}{\partial u} - D \cdot \frac{\partial u}{\partial u \partial x} \right) u_x \sim v \cdot u_x \quad (28)$$

$$u_t = p - f_x \text{ (Eq 20)} \quad f_t = \frac{\partial f}{\partial u} \cdot \frac{\partial u}{\partial t} = \left(v \cdot \frac{\partial u}{\partial u} - D \cdot \frac{\partial u}{\partial u \partial x} \right) u_t \sim v \cdot u_t \quad (29)$$

367 This set of equations prove that only u and u_x are needed to solve Eq 25. There are many
368 possibilities to calculate the derivative u_x from u . In the present model, it was calculated by
369 using a modified harmonic mean [37]:

$$u_x = \frac{|u_x^+|u_x^- + |u_x^-|u_x^+}{|u_x^+| + |u_x^-|} \quad u_x^- = (u_j^n - u_{j-1}^n)/\Delta x \quad u_x^+ = (u_{j+1}^n - u_j^n)/\Delta x \quad (30)$$

370 where u_x^- and u_x^+ are the partial derivatives on the left and right sides, respectively. The
371 modified harmonic mean equals zero when u_x^- and u_x^+ have opposite signs and equals the
372 traditional harmonic mean when u_x^- and u_x^+ have the same sign.

373 Thus, only one variable u is needed to solve the system, which is calculated via Eq 25 with an
374 explicit scheme. Starting from points at time step n , Eqs 22–30 allow us to move to time step
375 $n+1/2$. Points at time $n+1$ are then calculated in the same way as points at time $n+1/2$.

376 Meanwhile, the mass balance in the stationary phase can be solved separately by a 1st order
377 finite-difference method, at each mesh point (j,n):

$$\frac{q_j^n - q_j^{n-1}}{\Delta t} = k_a \cdot (q^{eqj} - q_j^n) \quad (31)$$

378 Boundary conditions are used to obtain values of first and last mesh points, as proposed by
379 Chuanyi et al. [37]:

$$\frac{\partial c_1^n}{\partial x} \sim \frac{c_2^n - c_1^n}{\Delta x} = \frac{v}{D} (c_1^n - c_{feed}) \quad (32)$$

$$\frac{\partial c_{j_{end}}^n}{\partial x} \sim \frac{c_{j_{end}}^n - c_{(j_{end}-1)}^n}{\Delta x} = 0 \quad (33)$$

380 3. Results and discussion

381 3.1 Influence of Langmuir and ion-exchange coefficients

382 A tailing can be observed in the chromatography outlet profile of some organic acids with a
383 strong anionic exchange resin. Theoretically, this could be due to a high value of their
384 adsorption affinity k_s or ion-exchange coefficient K^{iex} . Figures 6-A and 6-B show the impact
385 of values k_s and K^{iex} on the outlet profile during the single component pulse test simulation
386 of citric acid with parameters of Tables 4, 5 and 7. In Figure 6-A, K^{iex} is fixed at 1, a
387 negligible value, to study only the influence of k_s on the profile shape and position. Then,
388 the influence of K^{iex} is depicted in Figure 6-B. Pulse tests with different values of K^{iex} were
389 simulated. As the objective was to highlight the effect of K^{iex} only on the profile shape, the
390 value of k_s was adjusted for each value of K^{iex} to obtain the same retention volume.

391 As expected, Figure 6-A shows that the higher is the adsorption coefficient k_s , the higher is
392 the retention volume. However, the value of the coefficient k_s barely changes the profile
393 shape and its relative symmetry. In comparison, Figure 6-B shows that K^{iex} significantly
394 impacts the profile shape by increasing its tailing.

395 To summarize, the retention volume depends on both K^{iex} and k_s while the profile tail is
396 influenced almost solely by K^{iex} . Indeed, very high k_s values could also lead theoretically to
397 significant profile tailing, but these values would not be consistent with experimental
398 retention volume, which corresponds to a k_s ranging between 0 and 0.3 L/mol.

399 The impact of ion-exchange constant K^{iex} depends on the pH of the liquid phase and the
400 pKa of the organic acid. When the pH is much lower than pKa ($\text{pH} < \text{pKa} - 2$), organic acids
401 are mainly in molecular form. In this case, a very small proportion is dissociated into the
402 anionic form, and the peak is less sensitive to the value of K^{iex} .

403 3.2 Identification of Langmuir and ion-exchange coefficients

404 In the present study, K^{iex} was estimated to reproduce the experimental profile tailing
405 obtained for formic, succinic, and citric acids, starting from the resin supplier's estimation.
406 Meanwhile, k_s was adjusted to fit the experimental retention volume. Initially, k_s was set to
407 the experimental value estimated previously from equilibrium curves, considering different
408 possible N values (Table 4). Figure 7 shows experimental mono-component pulse tests that
409 were used to refine estimations of k_s and K^{iex} given in Table 6. The operating conditions of
410 these pulse tests are detailed in Table 5.

411 The mean value of D obtained from the van Deemter curve was used for simulation. Only
412 the value of k_a was slightly adjusted to fit better the peak left front (Table 7).

413 In Table 6, the identified ranges of K^{iex} correspond quite well to the supplier's data for
414 formic and citric acids. k_s ranges identified from pulse test simulations were not influenced
415 by different possible N values considered for each organic acid. Indeed, the denominator
416 $(1 + N \cdot k_s \cdot c)$ of the Langmuir equation remained close to 1 because of weak component
417 concentration during pulse test simulations. For formic and succinic acids, the k_s range
418 estimated from pulse test simulation is consistent with its range identified from equilibrium
419 curves, for $N = 0.5$ and 4, respectively. Meanwhile, the k_s range of citric acid identified from
420 pulse tests lies at the bottom of its range estimated from equilibrium curves. Thus, 0.5, 4
421 and 8 were considered afterward as the unique, consistent N values for formic, succinic and
422 citric acids, respectively. For citric acid, the slight k_s overestimation from equilibrium curves

423 can be explained by the strong influence of ion-exchange (illustrated by the significant tailing
424 of the citric acid profile, cf. Fig. 7).

425 3.3 Analysis of ion-exchange effect on the chromatography profile

426 Figure 7 presents simulation curves of pulse tests for different organic acids, to compare the
427 Langmuir adsorption model with the hybrid model, which considers that organic acid can be
428 retained by Langmuir adsorption but also by ion-exchange.

429 Both models can predict the experimental results for formic acid. This is not surprising as its
430 tailing is negligible, and its profile is almost symmetrical. The formic acid profile is marginally
431 influenced by ion-exchange due to its very low K^{iex} (< 30). Moreover, it is much less
432 dissociated into anions than citric acid because of its higher pKa (3.76 vs. 3.13). Thus, at pH
433 1.5, only 0.5% formic acid is dissociated, making the ion-exchange effect even more
434 negligible.

435 In comparison, succinic acid has the highest pKa (4.16) but also the highest K^{iex} according to
436 Table 6 (900 ± 100). Therefore, despite a low proportion dissociated into anions (0.2% at pH
437 1.5), the strong retention of succinate anion on resin ion-exchange sites can explain its slight
438 profile tailing.

439 Finally, the citric acid profile has the largest tailing because of its lower pKa (3.13) and quite
440 high K^{iex} . Indeed, citric acid is the most dissociated into anions (2.3% at pH 1.5) and citrate
441 anions are strongly retained by ion-exchange.

442 Figure 7 confirms that the tailing of succinic and citric acid profiles cannot be reproduced by
443 the Langmuir adsorption model. In contrast, the hybrid model is in good agreement with
444 experimental results. It confirms that organic anions retention by ion-exchange must be
445 considered to make predictive simulation, even if they are poorly dissociated at pH = 1.5.

446 4. Multi-component pulse test prediction

447 To confirm that the hybrid model is more predictive than the model with only Langmuir
448 adsorption, a pulse test with a mixture of formic acid and succinic acid was both simulated
449 and carried out (Fig. 8). Table 8 gives parameter values used in both models, whose ranges
450 were estimated previously from experimental data analysis (Tables 6 and 7).

451 Experimental profiles depicted in Figure 10 correspond to a pulse test performed with 10 mL
452 pH 1.5 solution, composed of 0.65 mol/L formic acid and 0.267 mol/L succinic acid, eluted
453 with pH 1.5 H_2SO_4 solution at 0.5 BV/h, using the same setup described above.

454 Figure 8 confirms clearly that the hybrid model predicts the chromatographic profile of both
455 organic acids much better. More specifically, the hybrid model is able to predict the
456 significant tailing of the succinic acid profile, unlike the Langmuir model. Moreover, the
457 mean retention volume of formic acid is better predicted by the hybrid model, even though
458 there is still a slight difference (0.1 BV) compared to experimental points.

459 The slight discrepancies observed can be due to assumptions and simplifications in the
460 present hybrid model. For example, all adsorption sites were considered equivalent. To be
461 more accurate, adsorption sites on the upper side of SO_4^{2-} and HSO_4^- counter-anions
462 should be considered more accessible than sites closer to the resin matrix (Fig. 4). In
463 addition, some studies [38, 39] showed that the original Langmuir competitive equation is

464 not suitable for multi-layer adsorption. Thus, a more accurate model considering different
465 types of adsorption sites might be an interesting approach to better predictions of multi-
466 component mixture separation by chromatography.

467 5. Conclusion

468 Strong anionic resins, often used in sulfate form in chemical or food and feed industries to
469 separate organic acids by chromatography, require better retention mechanisms to improve
470 the model's prediction. In this work, a hybrid model was developed and used to explain the
471 elution profiles of succinic and citric acids, which display unusual tailing. Compared to classic
472 Langmuir adsorption models, it also considers the effect of organic acid dissociation into
473 anions that can be retained on resin ion-exchange sites. The model was solved with the
474 CE/SE method.

475 Estimation of adsorption equilibrium coefficient (N and k_s) were consistent with the
476 adsorption of organic acids by means of hydrogen bonding between the hydrogen atom of
477 the carboxylic acid group and one lone electron pair of oxygen atoms of sulfate or hydrogen
478 sulfate counter-anions. Present results confirm that the tailing of succinic and citric acid
479 profiles is mainly caused by ion-exchange of their very low dissociated fraction, even at low
480 pH (< 1.5). Organic acid dissociation and ion-exchange is, therefore, must be considered to
481 develop a predictive model for succinic and citric acids. The prediction of the hybrid model
482 was successfully validated in the case of a multi-component pulse test.

483 This hybrid model is currently implemented in a multi-column chromatography simulation
484 program to predict and optimize the performance of simulated moving bed technologies. It
485 is also useful to design new multi-fraction processes.

486

487 Acknowledgments

488 This study was carried out in the Centre Européen de Biotechnologie et de Bioéconomie
489 (CEBB), supported by Région Grand Est, Département de la Marne, Grand Reims and the
490 European Union. In particular, the authors would like to thank Département de la Marne,
491 Grand Reims, Région Grand Est and European Union with European Regional Development
492 Fund (ERDF Champagne-Ardenne 2014-2020) for their financial support to the Chair of
493 Biotechnology of CentraleSupélec.

494 References

- 495 [1] Jun Y., Feijie H., Wenyan H., Method for detecting paraffin in food by gas
496 chromatography and gas chromatography-mass spectrometry and application
497 thereof, Worldwide applications, CN Patent 102621245A, 2012
- 498 [2] Shane M.P., Methods for monitoring integrated continuous pharmaceutical
499 manufacturing processes, US Patent 20160041551A1, 2016,
- 500 [3] Qiao-Le H., Zhao-xi S., Liming Z., Model-based process design of a ternary protein
501 separation using multi-step gradient ion-exchange SMB chromatography, Computers
502 & Chemical Engineering 138 (2020), [https://doi.org/10.1016/j.compchemeng.-](https://doi.org/10.1016/j.compchemeng.-2020.106851)
503 2020.106851

- 504 [4] Ammann, A.A. Speciation of heavy metals in environmental water by ion
505 chromatography coupled to ICP–MS, *Anal Bioanal Chem* 372 (2002), 448–452,
506 <https://doi.org/10.1007/s00216-001-1115-8>
- 507 [5] Kaifei C., Shilai H., Hang L., Gang L., Shicheng Z.g, Jian-min C., Ion exchange
508 separation for recovery of monosaccharides, organic acids and phenolic compounds
509 from hydrolysates of lignocellulosic biomass, *Separation and Purification Technology*
510 172 (2017), 100-106, <https://doi.org/10.1016/j.seppur.-2016.08.004>
- 511 [6] Bolin G., Lili W., Chaozhan W., Xindu G., Preparation of hydrophobic interaction
512 chromatographic packings based on monodisperse poly (glycidyl-methacrylate-co-
513 ethylenedimethacrylate) beads and their application, *Journal of Chromatography A*
514 1022 (2004), 33-39 <https://doi.org/10.1016/j.chroma.-2003.09.063>
- 515 [7] Shanshan S., Xiulan X., Lijun Z., Liang C., Zhaochu X., Yufeng L., Preparative
516 separation of five polyphenols from the fruits of *Sorbus pohuashanensis* Hedl. by
517 high-speed counter-current chromatography, *Journal of Chromatography B* 1172
518 (2021), <https://doi.org/10.1016/j.jchromb.2021.122620>.
- 519 [8] Ton B., Pascal B., Peter J.S., Ron A.H. Peters, Charge-based separation of synthetic
520 macromolecules by non-aqueous ion exchange chromatography, *Journal of*
521 *Chromatography A* 1626 (2020), <https://doi.org/10.1016/j.chroma.2020.461351>.
- 522 [9] Ali S., Mohammad Reza K., Masoud A., Ahmad S., Shahram S., Mathematical
523 modeling and optimization of industrial scale ELUXYL simulated moving bed (SMB),
524 *Separation and Purification Technology* 248 (2020), [https://doi.org/10.1016/-](https://doi.org/10.1016/-j.seppur.2020.116961)
525 [j.seppur.2020.116961](https://doi.org/10.1016/-j.seppur.2020.116961).
- 526 [10] Cheol-Yeon J., Jae-Hwan C., Jin-Woo K., Sungyong M., Development of a simulated
527 moving bed process for ultra-high-purity separation of ribose from a low-selectivity
528 sugar mixture in microalgal hydrolyzate, *Separation and Purification Technology* 262
529 (2021), <https://doi.org/10.1016/-j.seppur.2020.118298>
- 530 [11] Julien L., Claire-Line B., Florence L., Marc-André T., Moncef S., Dominique P.,
531 Purification of organic acids by chromatography with strong anionic resins:
532 Investigation of uptake mechanisms; *Journal of Chromatography A* 1458 (2016), 63-
533 69, <https://doi.org/10.1016/j.chroma.-2016.06.057>.
- 534 [12] Kulprathipanja S., Oroskar A.R., Separation of lactic acid from fermentation broth
535 with an anionic polymeric absorbent, US Patent 5068418, 1991.
- 536 [13] Guiochon G., Shirazi D.G., Felinger A., Katti A.M., Fundamentals of preparative and
537 non-linear chromatography, Academic Press 2nd edition (2006), 283–286,
538 ISBN0123705371, 9780123705372.
- 539 [14] Juke, A., Epping, A., Schmidt-Traub, H., Optimal design of batch and simulated
540 moving bed chromatographic separation processes, *Journal of Chromatography A*
541 944 (2012), 93-117, [https://doi.org/10.1016/S0021-9673\(01\)01311-5](https://doi.org/10.1016/S0021-9673(01)01311-5).
- 542 [15] Kaczmarek K., Use of orthogonal collocation on finite elements with moving
543 boundaries in the simulation of non-linear multi-component chromatography.
544 Influence of fluid velocity variation on retention time in LC and HPLC, *Computers &*
545 *Chemical Engineering* 20 (1996), 49-64, [https://doi.org/10.1016/0098-](https://doi.org/10.1016/0098-1354(95)00004-L)
546 [1354\(95\)00004-L](https://doi.org/10.1016/0098-1354(95)00004-L).
- 547 [16] Hørsholt A., Christiansen L.H., Meyer K., Huusom J.K., Jørgensen J.B., A
548 Discontinuous-Galerkin Finite-element method for simulation of packed bed
549 chromatographic processes, *FAC-PapersOnLine* 52 (2019), 346-351,
550 <https://doi.org/10.1016/-j.ifacol.2019.06.086>.

- 551 [17] Dünnebieer G., Weirich I., Klat K.U.t, Computationally efficient dynamic modelling and
552 simulation of simulated moving bed chromatographic processes with linear
553 isotherms, *Chemical Engineering Science* 53 (1998), 2537-2546,
554 [https://doi.org/10.1016/S0009-2509\(98\)00076-1](https://doi.org/10.1016/S0009-2509(98)00076-1).
- 555 [18] Kaczmarski K., Antos D., Fast finite difference method for solving multi-component
556 adsorption-chromatography models, *Computers & Chemical Engineering* 20 (1996),
557 1271-1276, [https://doi.org/10.1016-/0098-1354\(95\)00247-2](https://doi.org/10.1016-/0098-1354(95)00247-2).
- 558 [19] Lim Y.I., Le Lann J.M., Joulia X., Accuracy, temporal performance and stability
559 comparisons of discretization methods for the solution of partial differential
560 equations (PDEs) in the presence of steep moving fronts, *Computers and Chemical
561 Engineering*, 25 (2001), 1483-1492, [https://doi.org/10.1016/S0098-1354\(01\)00712-8](https://doi.org/10.1016/S0098-1354(01)00712-8).
- 562 [20] Chang, S.C., The method of space-time conservation element and solution
563 element—A new approach for solving the navier-stokes and euler equations. *J.
564 Comput. Phys.* 119, 2 (July 1995), 295–324. <https://doi.org/10.1006/-jcph.1995.1137>
- 565 [21] Wei L., Dong H., Pan H., Hu X., Zhu J., Study on the mechanism of the deflagration to
566 detonation transition process of explosive, *Journal of Energetic Materials* 32 (2014)
567 238-251. <https://doi.org/10.1080/07370652.2013.825347>
- 568 [22] Shen H., Gang W., Liu K., Deliang Z. Numerical simulation of liquid-fueled
569 detonations by an eulerian-lagrangian model. *International Journal of Nonlinear
570 Sciences and Numerical Simulation* (2012), 13, [https://doi.org/177-188.
571 10.1515/ijnsns.2011.102](https://doi.org/177-188.10.1515/ijnsns.2011.102).
- 572 [23] Orkomi A.A., Shahrokhi M., Simulation and control of multidimensional
573 crystallization processes, *Chem. Eng. Commun.* 201 (2014), 870-895,
574 <https://doi.org/10.1080-/00986445.2013.785947>.
- 575 [24] Qamar S., Yousaf M., The space-time CESE method for solving special relativistic
576 hydrodynamic equations, *J. Comput. Phys.* 231 (2012) 3928-3945, [https://doi.org/-
577 10.1016/j.jcp.2012.01.039](https://doi.org/-10.1016/j.jcp.2012.01.039).
- 578 [25] Sadighi S., Ahmad A., Shirvani M., Dynamic simulation of a pilot scale vacuum gas oil
579 hydrocracking unit by the space-time CE/SE method, *Chemical Engineering &
580 Technology* 35 (2012), 919-928, <https://doi.org/10.1002/ceat.201100305>
- 581 [26] Young-II L., Sten-Bay J., A fast and accurate numerical method for solving simulated
582 moving bed (SMB) chromatographic separation problems, *Chemical Engineering
583 Science*, Volume 59 (2004), 1931-1947, <https://doi.org/10.1016-/j.ces.2003.12.026>
- 584 [27] Lan L., Young-II L., Performance evaluation of the conservation element and solution
585 element method in SMB process simulation; *Chemical Engineering and Processing*
586 48 (2009), 878–884, <https://doi.org/10.1016/j.cep.2008.11.003>
- 587 [28] Van Deemter J. J., Zuiderweg F.J., Klinkenberg A., Longitudinal diffusion and
588 resistance to mass transfer as causes of nonideality in chromatography. *Chemical
589 Engineering Science* 50 (1995), 3869-3882, [https://doi.org/10.1016/00092509-
590 \(96\)81813-6](https://doi.org/10.1016/00092509-(96)81813-6).
- 591 [29] Felinger, A., Guiochon, G. Comparison of the kinetic models of linear
592 chromatography. *Chromatographia* 60 (2004), 175-180. [https://doi.org/10.1365-
593 /s10337-004-0288-7](https://doi.org/10.1365-/s10337-004-0288-7)
- 594 [30] Kulprathipanja S., Oroskar A.R., Separation of lactic acid from fermentation broth
595 with an anionic polymeric absorbent, US Patent 5068418, 1991.
- 596 [31] Kulprathipanja S., Oroskar A.R., Separation of an organic acid from fermentation
597 broth with an anionic polymeric adsorbent, US Patent 5068419, 1991.

- 598 [32] Sircar S., Comments on practical use of Langmuir gas adsorption isotherm model.
599 Adsorption 23 (2017), 121–130. <https://doi.org/10.1007/s10450-016-9839-0>
- 600 [33] Benni D., Weichao Z., Catalytic effect of water, water dimer, or formic acid on the
601 tautomerization of nitroguanidine, Computational and Theoretical Chemistry 1049
602 (2014), 90-96, <https://doi.org/10.1016/-j.comptc.2014.09.025>.
- 603 [34] Ion Exchange Resins Selectivity, DuPont, Form No. 45-D01458-en, Rev. 2 November
604 2019
- 605 [35] DOWEX™ Ion Exchange Resins Technical Information, Form No. 177-01755-0207
- 606 [36] Sin-Chung C., "Courant Number and Mach Number Insensitive CE/SE Euler Solvers,"
607 AIAA Paper 2005-4355, 41st AIAA/ASME/SAE/ASEE Joint Propulsion Conference and
608 Exhibit (2005), Tucson, AZ.
- 609 [37] Chuanyi Y., Shaokun T., Yinghua L., Hong-Mei Y., Moses O.T., Combination of space–
610 time conservation element/solution element method and continuous prediction
611 technique for accelerated simulation of simulated moving bed chromatography,
612 Chemical Engineering and Processing: Process Intensification 96 (2015), 54-61,
613 <https://doi.org/10.1016/-j.cep.2015.07.023>.
- 614 [38] Neil R.A., Adsorption of formic acid on clean and oxygen covered Pt(111),
615 Applications of Surface Science 11-12 (1982), 774-783,
616 [https://doi.org/10.1016/0378-5963\(82\)90120-9](https://doi.org/10.1016/0378-5963(82)90120-9).
- 617 [39] Nejad A., Suhm M., Concerted Pair Motion Due to Double Hydrogen Bonding: The
618 Formic Acid Dimer Case, Journal of the Indian Institute of Science 100 (2019),
619 <https://doi.org/100.10.1007/s41745-019-00137-5>.

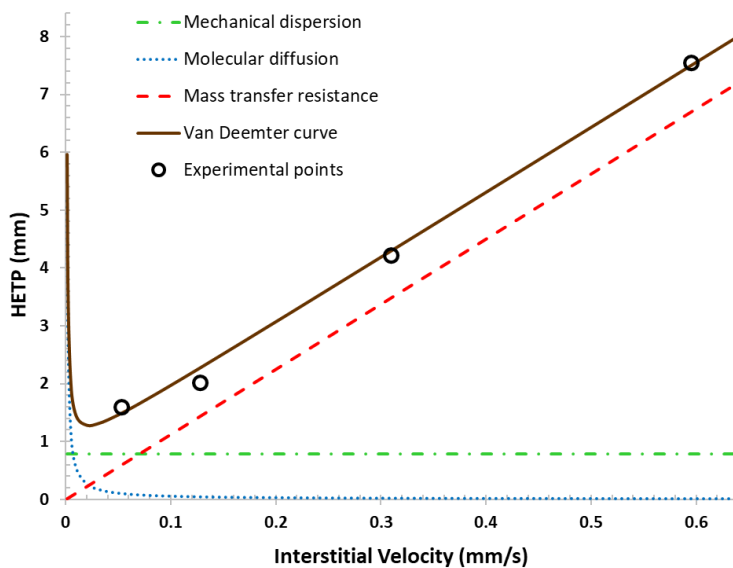
620 Appendices

621 SBA (strong base anion) resins selectivity coefficients [34, 35]

Anion	Type 1	Type 2
$HSiO_3^-$	<1.0	<1.0
OH^-	1.0	1.0
F^-	1.6	0.3
$CH_3CH_2COO^-$	2.6	0.3
CH_3COO^-	3.2	0.5
$HCOO^-$	4.6	0.5
$H_2PO_4^-$	5.0	0.5
IO_3^-	5.5	0.5
HCO_3^-	6.0	1.2
Cl^-	22	2.3
NO_2^-	24	3
BrO_3^-	27	3
HSO_3^-	27	3
CN^-	28	3
HSO_4^-	35	9
Br^-	50	6
NO_3^-	65	8
ClO_3^-	74	12
Phenate	110	27
SO_4^{2-}	150	/
I^-	175	17
SeO_4^{2-}	280	/
Citrate	220	23
ClO_4^-	>500	/
CrO_4^{2-}	1700	/
$C_6H_5SO_3^-$	>500	75

622

624

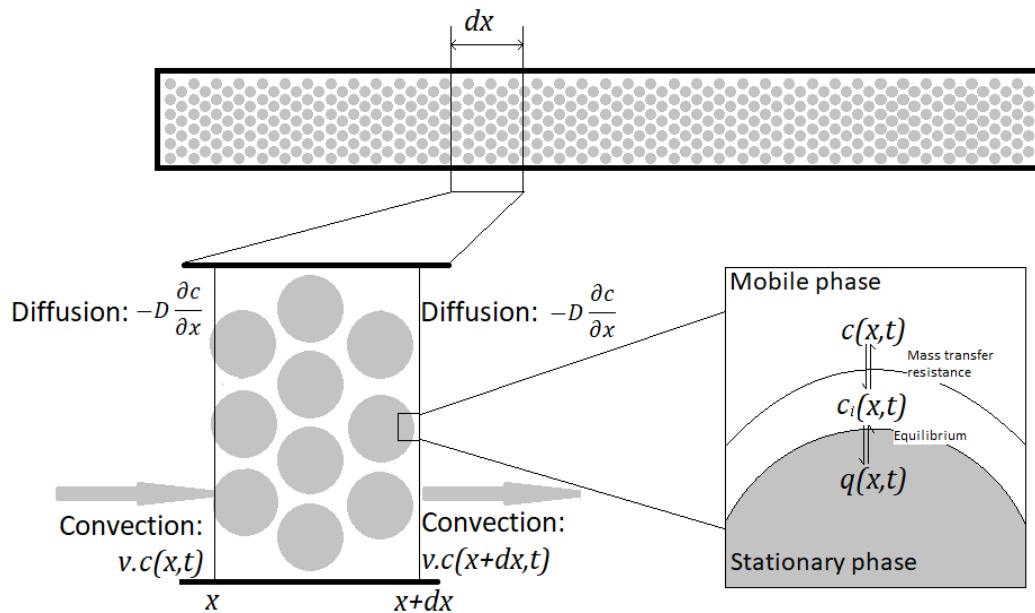


625

626 **Fig. 1.** van Deemter Curve of succinic acid eluted with H₂SO₄ solution at pH 1.5 with the system described in
627 materials and methods.

628

629

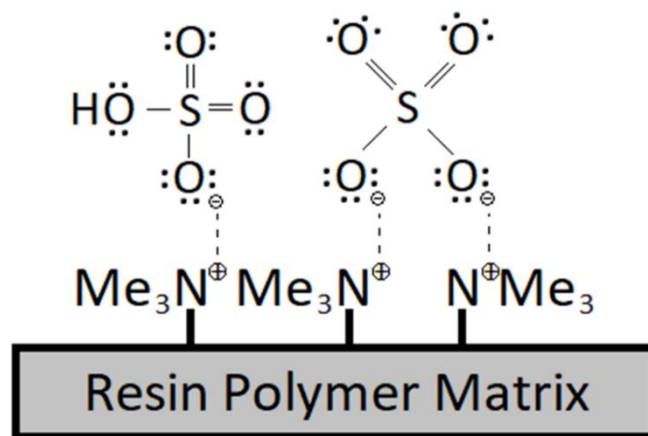


630

631

Fig. 2. Mass balance (convection-diffusion equation) and mass transfer model

632



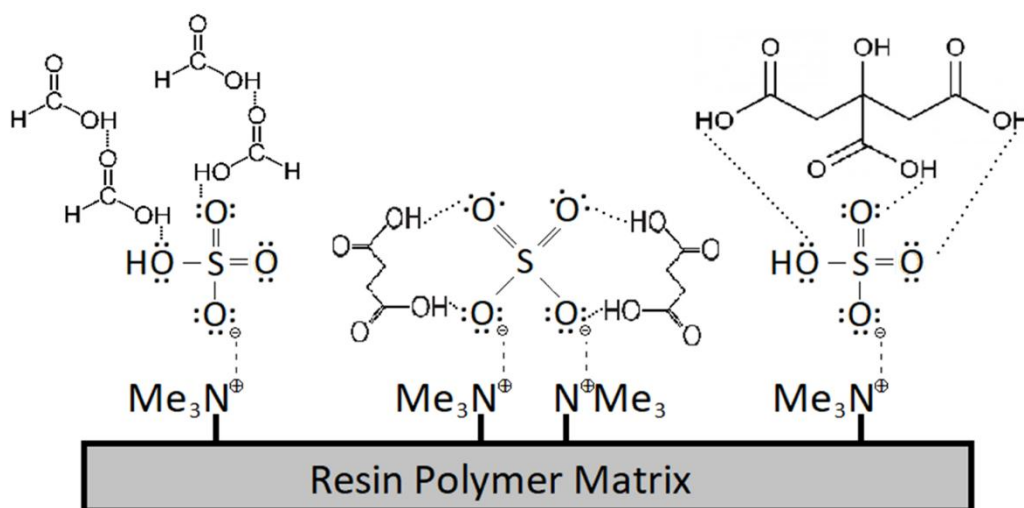
633

634

Fig. 3. Schematic representation of the strong anion resin (type 1) in sulfate form.

635

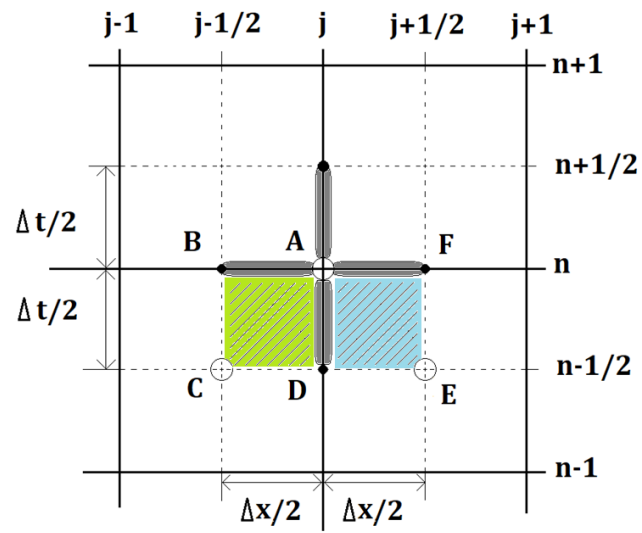
636



637

638 **Fig. 4.** Schematic illustration of organic acid adsorption by hydrogen bonding on SO_4^{2-} or HSO_4^- counter-anions,
639 which have eight lone electron pairs each. $N = 0.5$ for formic acid could be explained by dimer conformation, and
640 means that up to 16 molecules could be adsorbed (only 4 of them are represented). $N = 8$ for citric acid
641 corresponds to one molecule maximum adsorbed on each counter-anion. Indeed, citric acid can form up to 3
642 hydrogen bonds and the other five free sites could be cluttered. $N = 4$ for succinic acid corresponds to 2
643 molecules maximum adsorbed on each counter-anion, because it can form up to 2 hydrogen bonds and could
644 clutter less free sites.

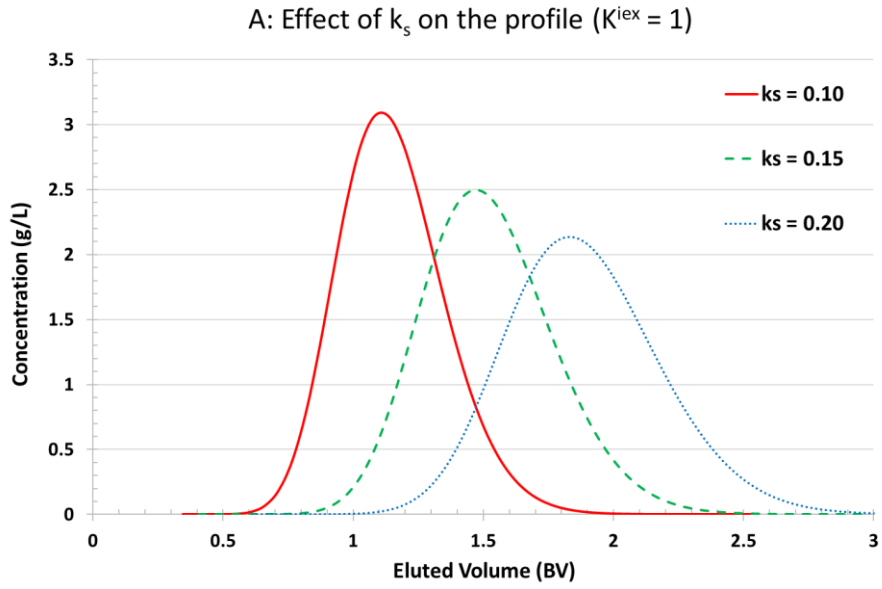
645



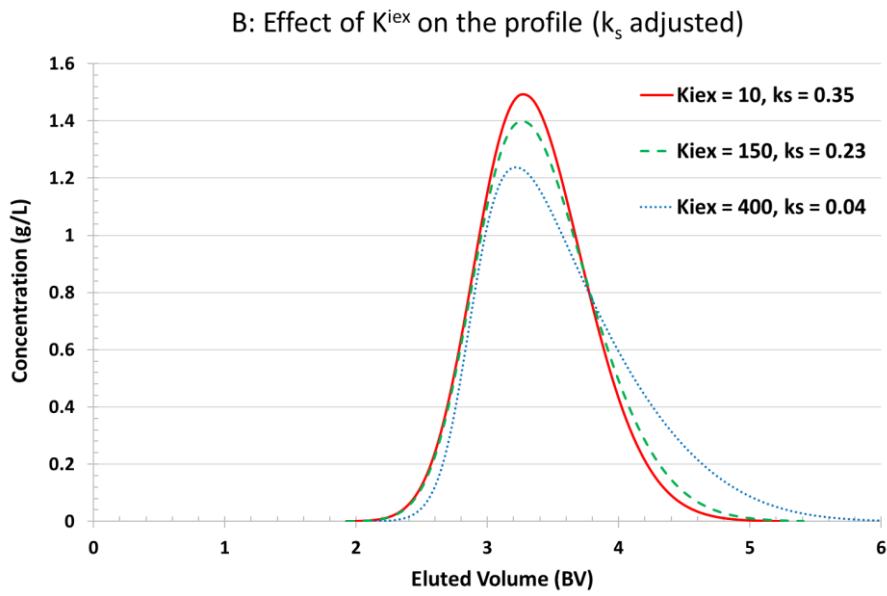
646

647 **Fig. 5.** The SE (solution element, gray part) and CE (conservation element, green and blue part) at position j and
 648 time n . Values at point A are calculated from points C and E at $n-1/2$; values at C or E are obtained from points at
 649 time $n-1$ via the CE and SE at the point at time $n-1/2$.

650



651

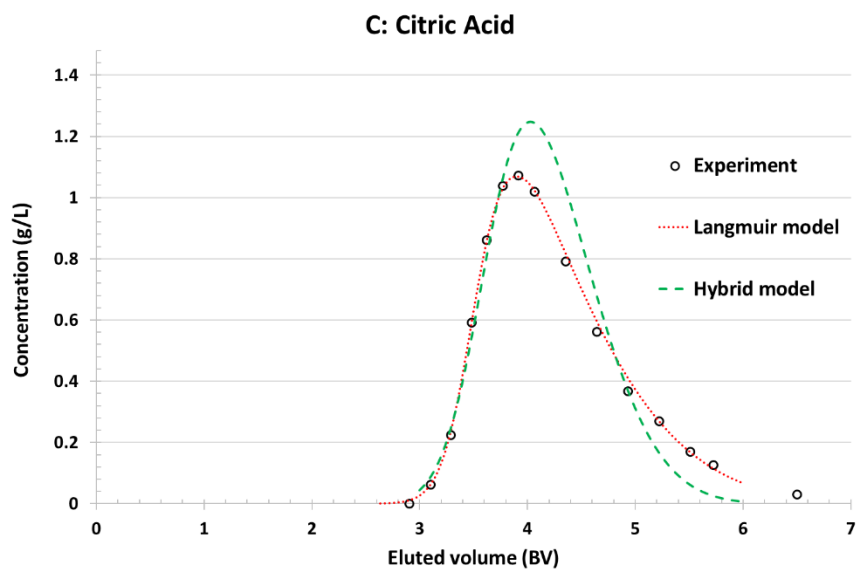
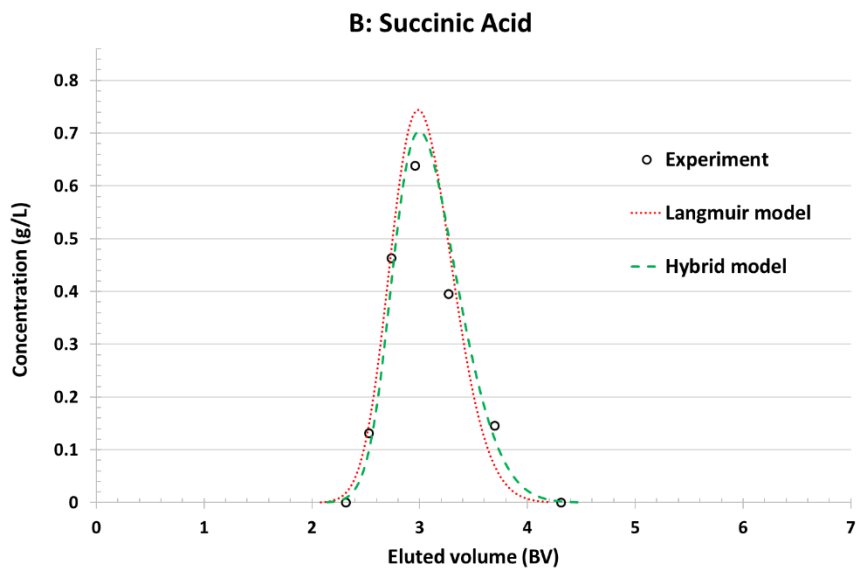
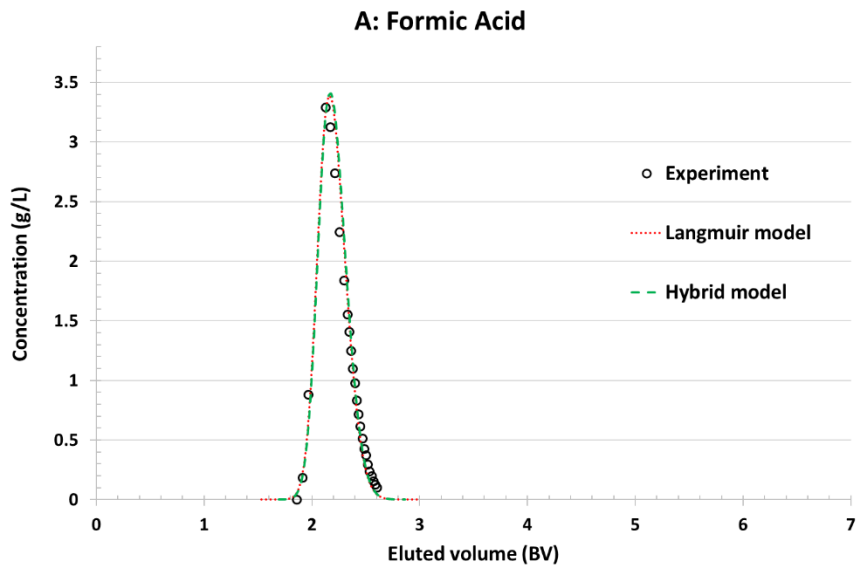


652

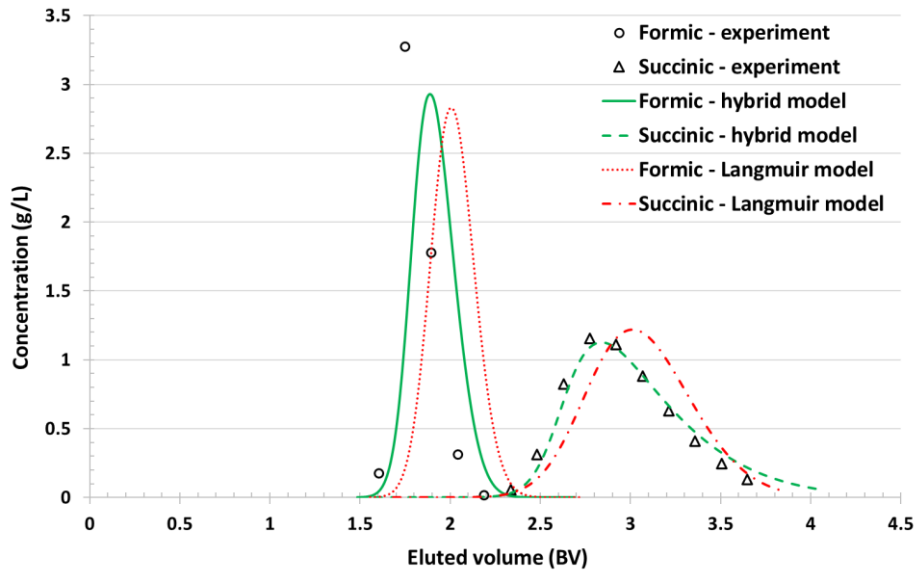
653

Fig. 6. Influence of k_s (Fig.6-A on the top) and K^{iex} (Fig.6-B at the bottom) on organic acid outlet profile.

654



658 **Fig.7.** Influence of ion-exchange on outlet profile of formic (Fig. 7-A), succinic (Fig. 7-B) and citric acids (Fig. 7-C)



659

660

661

Fig.8. Multi-component pulse test to compare predictions of a model with only Langmuir adsorption to the hybrid model, which also considers ion-exchange

662

663

664 **Table 1: Chemicals used in this work**

	Producer	N° CAS	Purity
Formic acid	Sigma-Aldrich	64-18-6	>98%
Succinic acid	Acros Organics	110-15-6	99%
Citric acid	Acros Organics	5949-29-1	99.5%
Sulfuric acid	VWR PROLABO	7664-93-9	95%
Na ₂ SO ₄	Acros Organics	7757-82-6	99+%

665

666 **Table 2: Devices used in this work**

Device	Manufacturer	Model
Pump	MasterFlex L/S	7518-10
Column	YMC Europe ltd.	ECO25
pH/conductivity sensor	Gilson	Verity 1810
UV sensor	Gilson	159 UV-VIS
Fraction collector	Gilson	FC 203B
HPLC	Dionex	Ultimate 3000

667

668 **Table 3: Main characteristics of the strong anionic resin used in this work (DIAION UMA 150)**

Matrix	Styrene-DVB Gel
Functional group	Quaternary ammonium (Type I)
Salt splitting capacity	> 1.4 eq/L
Water content	37–47%
Mean particle size	220–260 μm
Uniformity coefficient	< 1.1

669

670 **Table 4. Coefficients of the Langmuir equilibrium model for organic acid adsorption on HSO₄⁻ and**
671 **SO₄²⁻ counter-anions.**

Organic acids	<i>N</i> estimation	<i>N</i> assumed	<i>k_s</i> (L/mol)
Formic acid	0.25–1.15	0.5 or 1	0.05–0.25 (<i>N</i> = 0.5) 0.025–0.125 (<i>N</i> = 1)
Succinic acid	2.1–11	4 or 8	0.14–0.50 (<i>N</i> = 4) 0.07–0.25 (<i>N</i> = 8)
Citric acid	5.2–10	8	0.14–0.28

672

673

674 **Table 5. Operating conditions of single component pulse tests**

	Formic acid	Succinic acid	Citric acid
Sample volume (BV)	0.035	0.02	0.02
Concentration (mol/L)	0.75	0.27	0.55
Eluent	pH 1.5 H ₂ SO ₄ (0.02 mol/L)		
Flowrate (BV/h)	0.5		

675

676 **Table 6. Comparison of K^{iex} and k_s estimations of formic, succinic and citric acids**

Organic acid	K^{iex} identified from pulse test	K^{iex} supplier	k_s estimated from equilibrium curves	k_s identified from pulse test simulations
Formic acid	15 ± 10	5	0.05–0.25 ($N = 0.5$) 0.025–0.125 ($N = 1$)	0.2–0.25 ($N = 0.5$ or 1)
Succinic acid	900 ± 100	Not given	0.14–0.50 ($N = 4$) 0.07–0.25 ($N = 8$)	0.26–0.28 ($N = 4$ or 8)
Citric acid	300 ± 50	250	0.14–0.28 ($N = 8$)	0.12–0.14 ($N = 8$)

677

678 **Table 7. Values of k_a and D of formic, succinic and citric acids.**

Organic acid	k_a van Deemter (10^{-3} s^{-1})	k_a adjusted (10^{-3} s^{-1})	D van Deemter ($10^{-7} \text{ m}^2/\text{s}$)	D used ($10^{-7} \text{ m}^2/\text{s}$)
Formic acid	31–35	45	1–1.1	1
Succinic acid	7.5–9.5	8	0.68–1.4	0.8
Citric acid	2.8–3.4	5.6	4–5	4

679

680 **Table 8. Parameters used for multi-component pulse test simulation**

Model	Organic acid	N	k_s (L/mol)	K^{iex}	k_a (s^{-1})	D ($10^{-7} \text{ m}^2/\text{s}$)
Hybrid model (adsorption + ion-exchange)	Formic acid	0.5	0.24	25	0.045	1
	Succinic acid	4	0.26	800	0.008	0.5
Langmuir model (only adsorption)	Formic acid	0.5	0.25	0	0.045	1
	Succinic acid	4	0.44	0	0.008	0.5

681

682